Supporting Information

Wide Potential and High Energy Density for Asymmetric Aqueous-supercapacitor

Xinming Wu*, Bin Huang, Qiguan Wang,, Yan Wang

(School of Materials Science and Chemical Engineering, Xi'an Technological University, Xi'an 710032, P. R. China)

Measurements and Characterization

Morphology of the samples was investigated under JEOLJSM-6380LV (HITACHI) scanning electron microscope (SEM) at an accelerating voltage of 5 kV. Transmission electron microscope (TEM) micrographs were obtained with a HITACHI H-800, and all samples were treated by ultrasonic dispersion of ethanol solution before testing. The crystalline structure was carried out on a XRD-7000S/L diffractometer with a scan step of 6°. To determine the surface elemental compositions of the samples, the X-ray photoelectron spectra (XPS) was performed on X-ray AXIS Ultra-DLD photoelectron spectrometer using Al Kα X-rays as the excitation source.

Electrochemical performance measurements

Electrochemical performance evaluate were performed on an electrochemical workstation (Shanghai CH Instruments Co., CHI660E) in a three-electrode electrochemical cell using 1 M Na_2SO_4 aqueous solution as electrolyte at room temperature. The as-prepared samples were as the working electrode, while saturated calomel electrode (SCE) and a Pt mesh were used as the counter and reference electrodes, respectively. To test the electrode material of FG, one sheet of FG cut to 1

* Corresponding author: XM. Wu (✉), Tel: +8613720456279; fax: +86 29 88173324
. E-mail address: Aimar_wu@aliyun.com.

mm and were placed on the surface of a cellulose acetate membrane and immersed in 1 M HCl for 12 h to exchange their internal water and electrolyte. Then, the piece of the FG sheet was pressed against carbon cloth to separate the cellulose acetate membrane (labeled as FG-CC, Fig.S1). To get the electrochemically reduced FG-CC, the electrode was tested in 1 M Na_2SO_4 electrolyte for 100 CV cycles at 10 mV s^{-1} in the potential window of -1.4-0 V (labeled as Na-FG-CC, total load is about 103 mg). To test the electrode material of C@Mn_3O_4, C@Mn_3O_4 was mixed with PVDF, carbon black (increase electrical conductivity) in a ration of 8:1:1 with N-methyl-2-pyrrolidone. The mixture was grinded for 15 min to obtain slurry. The obtained-slurry was later coated onto carbon cloth which served as a current collector, and the dried at 80℃ overnight (labeled as C@Mn_3O_4-CC). To test the electrochemical performance, the C@Mn_3O_4-CC was directly cut to 2 cm × 4 cm (total load is about 112 mg) and used as the working electrode, saturated calomel electrode (SCE) was used as the reference electrode, and 1 M Na_2SO_4 aqueous solution as electrolyte. The asymmetric supercapacitor was characterized in a two-electrode cell configuration in 1 M Na_2SO_4 aqueous electrolyte. These two electrodes were subsequently assembled together with a filter paper as separator sandwiched in between. For all electrochemical performance, the measurement potential was controlled in the range of 0-2.7 V for aqueous electrolyte test. The CV was tested at current densities of 2, 5, 10, 20, and 50 mV s^{-1}, while the GCD was measured at current density of 1, 2, 5, 10, and 20 A g^{-1}. EIS test was measured in the measured in the frequency range from 0.01 to 10^6 Hz.

The specific capacitance, energy density and power density were calculated based on equation (1-3).

The specific capacitance of the samples was calculated from the charge-discharge curves based on the following equation:

$$F = (I \times \Delta t) / \Delta U \qquad (1)$$

where F(F g^{-1}) is the capacitance of the samples, I (A g^{-1}) refers to the discharge current; ΔU (V) is the potential window, Δt (s) is the discharge time.

The energy density and power density of the asymmetric supercapacitor can be

calculated from the galvanostatic charge-discharge curves via the following equation:

$$E = \frac{1}{2} \times F \times (\Delta U)^2 = (I \times \Delta t \times \Delta U) / (2 \times 3.6) \qquad (2)$$

$$P = 3600E / \Delta t \qquad (3)$$

where E is the energy density, P is the power density.

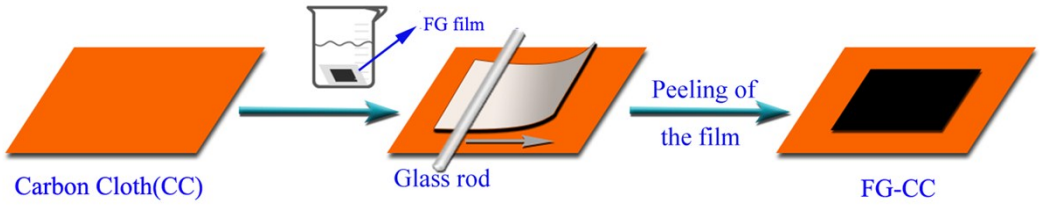

Fig. S1 Schematic illustration for the fabrication of FG-CC electrode

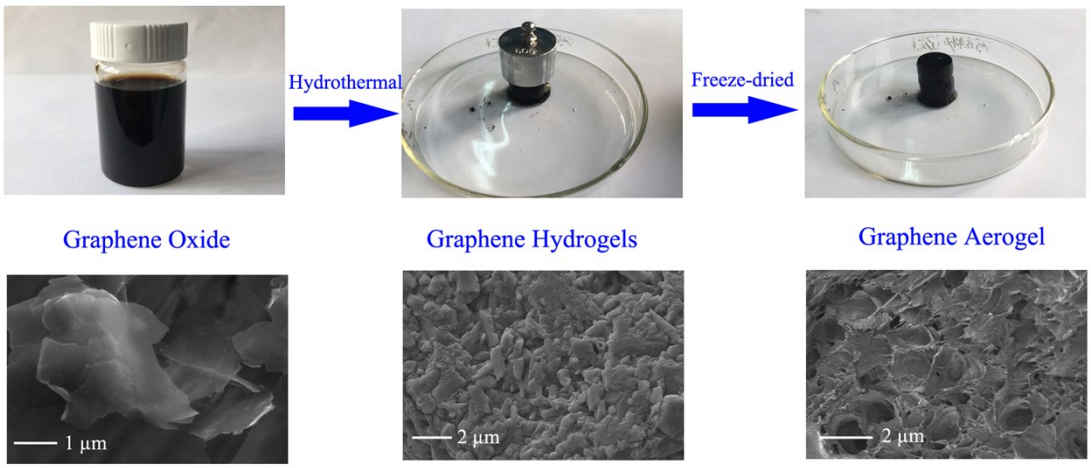

Fig. S2 Photographs of the preparation process and SEM of FG

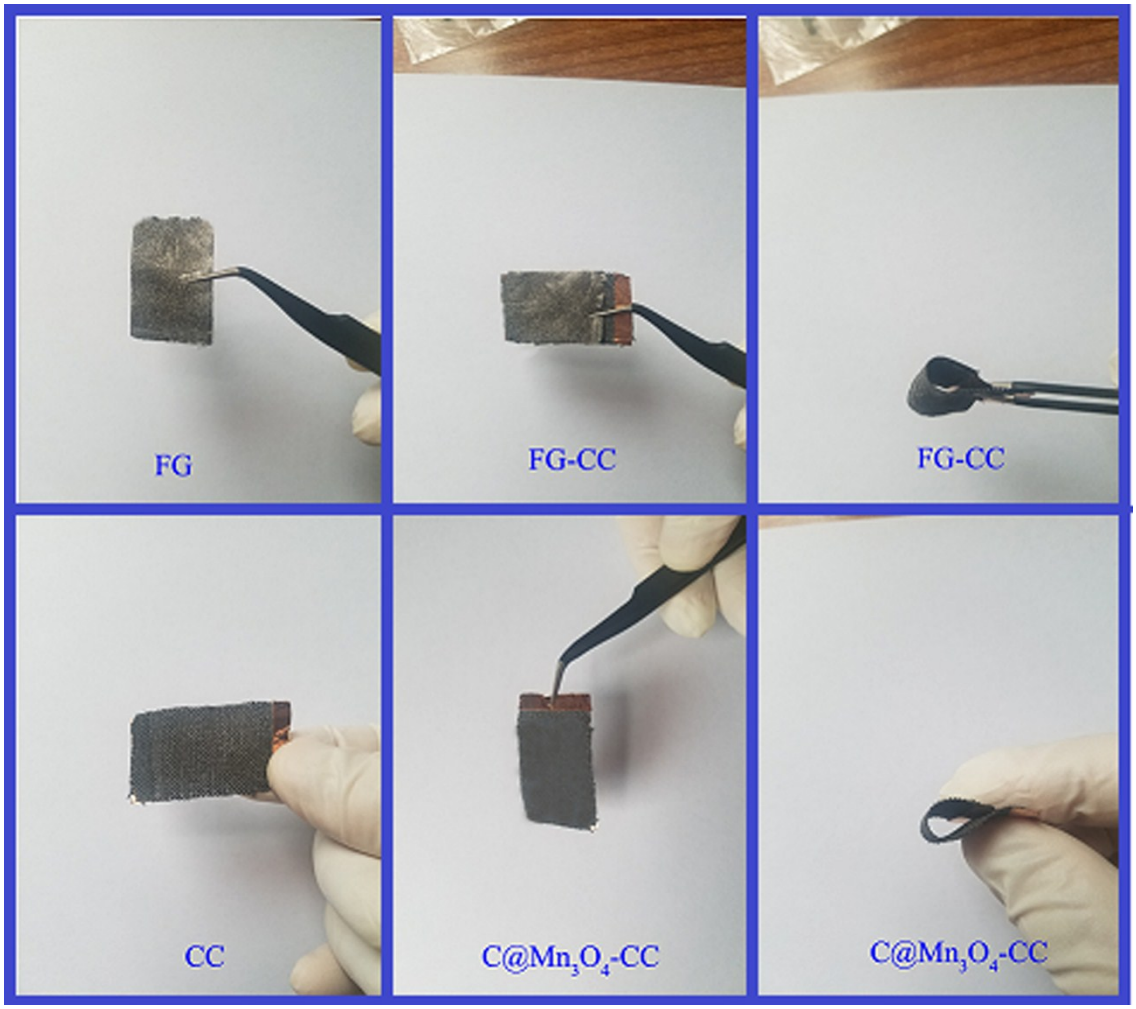

Fig. S3 Photographs of the FG-CC and C@Mn_3O_4-CC electrodes

$$\Delta G_{ads} = \Delta E_{ads} - T\Delta S_{ads}$$

$$\Delta E_{ads} = E_{FG+Na^+} - E_{Na^+} - E_{FG}$$

$$E_{Na^+} = E_{Na} + eU_{Na}$$

$$eU_{Na} = -2.94V\,(vs.SCE)$$

$$E_{Na} \approx DFT(G_{Na} + T\Delta S_{Na})$$

$$\Delta S_{ads} = S_{Na^+} - S^* - S_{Na}$$

$$S_{Na^+} - S^* = \text{harmonic approximation}$$

$$S_{Na} \approx 0$$

To compare the free energy of adsorption for Na^+ on different defects of FG, we utilized a method involving density functional theory (DFT) calculations of

adsorption energetic and use DMol^3 program in Materials Studio software. The electron exchange potential was treated by PW91 functional under the generalized gradient approximation (GGA). In the calculation, X and Y directions were taken to be in the graphene plane, Z direction was perpendicular to the graphene plane, and the vacuum layer was 20 Å. In the self-consistent iteration process, the simple brillouin region integral k points were selected 2×2×1 point by Monkhorst-Pack method, and the total energy error was no more than 1.0×10^{-4} Hartree. In the calculation, the spin was not limited, and the standard spin was selected as the initial spin. In the reciprocal k space, the orbital cut-off is selected as 5.1 Å. In all the calculations, FDT-D3 is used to deal with the van der Waals forces.

Lastly, although the effects of solvation energy and electric double layer are not considered, the relative adsorption strength of sodium for various defects in graphite is fully determined by our model. Relevant calculation results are shown in Table.S1.

Table.S1 Free energy of adsorption of Na^+ on different defect types in GF

Model	E_{total}**(keV)**	ΔE_{ads}**(eV)**	***D*(Å)**	$T\triangle S^*$	$\triangle G_{ads}$	***Illustration***
sp^2-C	-36.556	-0.612	2.28	0.072	-0.684	Fig.S4(a)
sp^3-C	-37.599	-0.835	2.54	0.124	-0.959	Fig.S4(b)
sp^3-O	-37.598	-0.810	2.06	0.085	-0.895	Fig.S4(c)

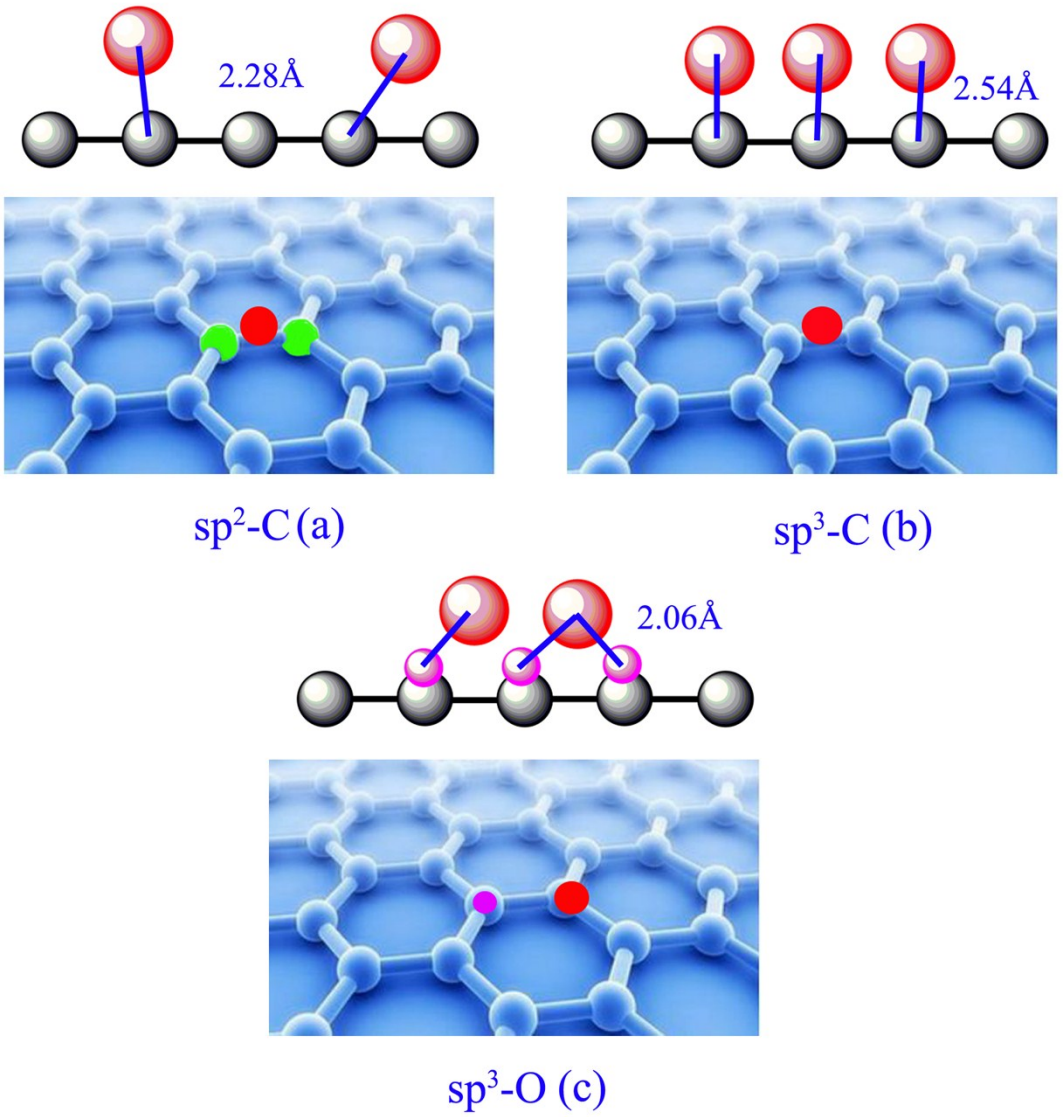

Fig. S4 Top and side views of Na^+ adsorbed on sp^2-C, sp^3-C, sp^3-O defects of FG

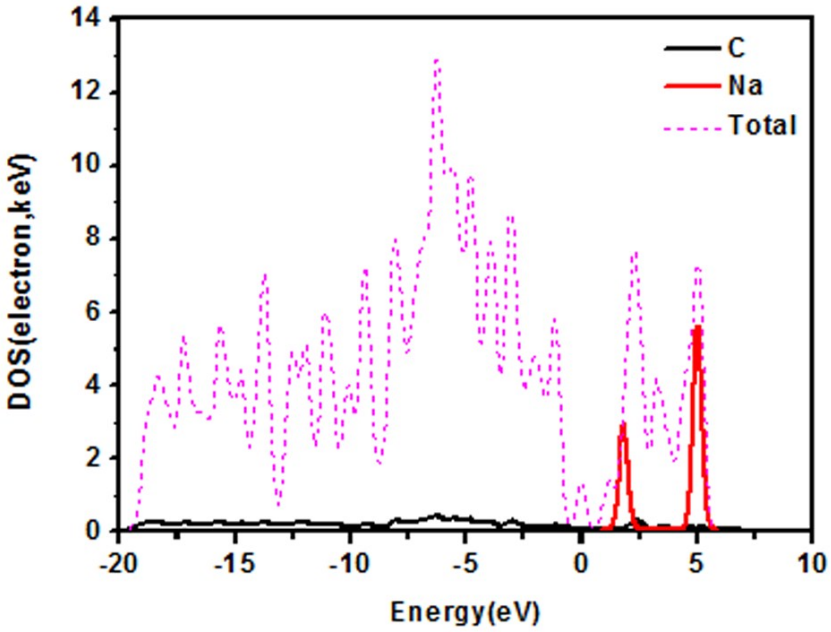

Fig.S5 The electronic densities of states (DOS) for FG after Na adsorption

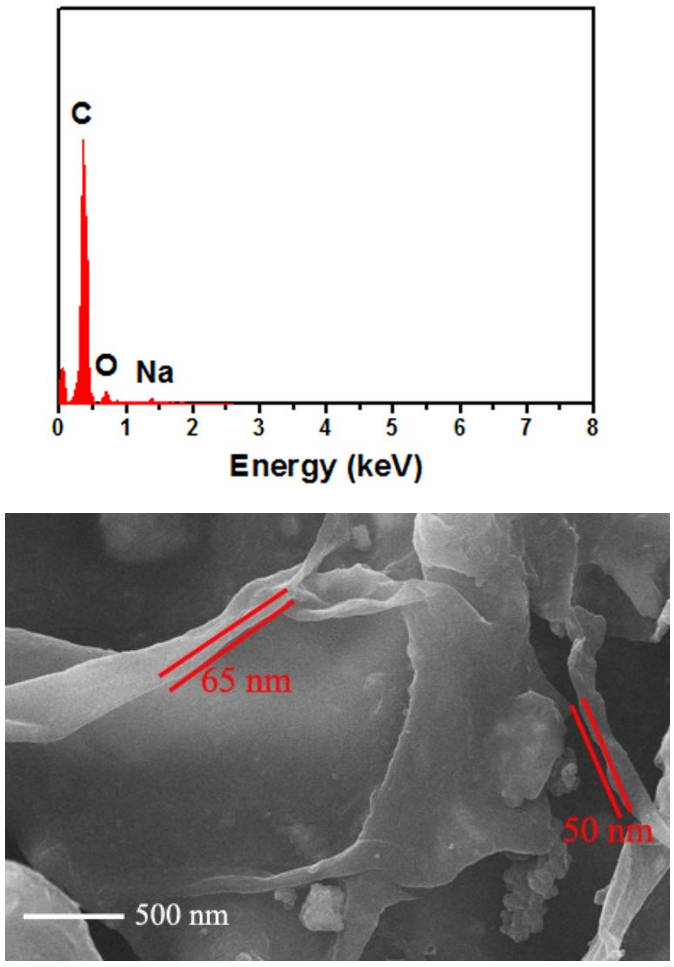

Fig.S6 EDX spectrum and high resolution SEM image of the Na-FG-CC

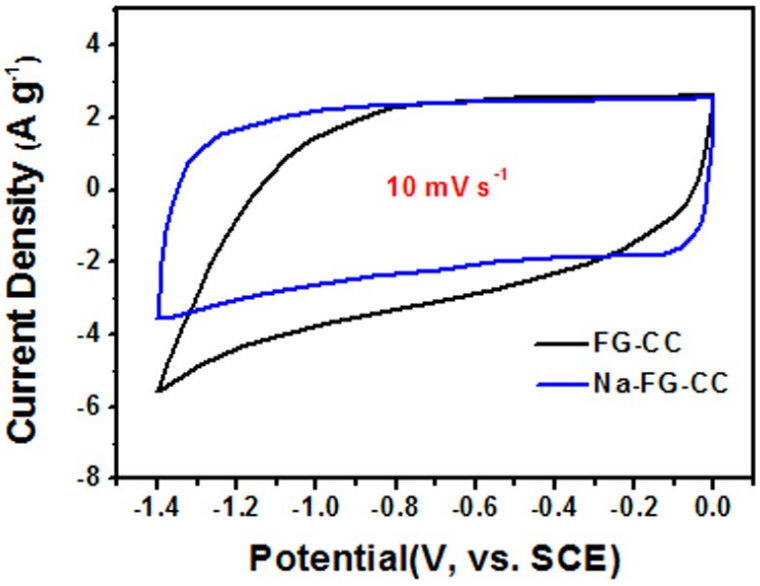

Fig.S7 CV curves of the FG-CC and Na-FG-CC (1 M Na_2SO_4 as electrolyte)

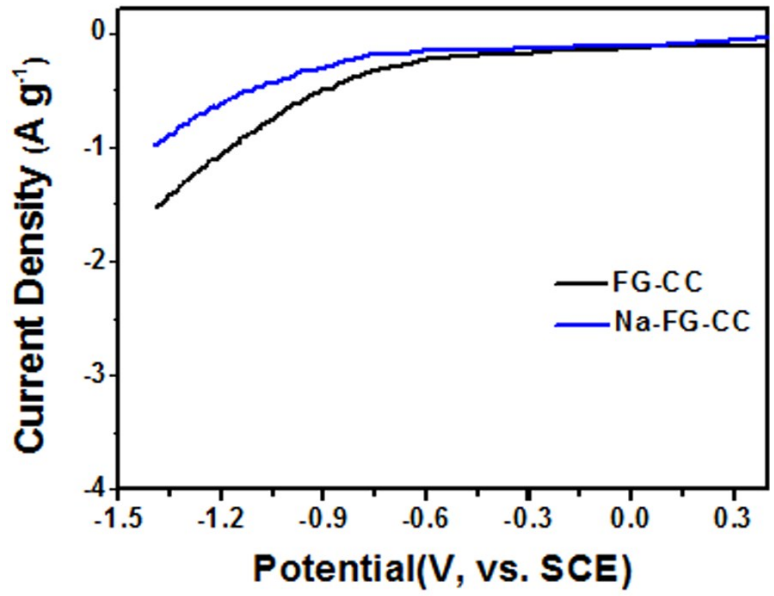

Fig.S8 Current density for the FG-CC and Na-FG-CC in 1 M Na_2SO_4 aqueous electrolyte at 5 mV s^{-1}, which reflects the standard potential for H_2 evolution.

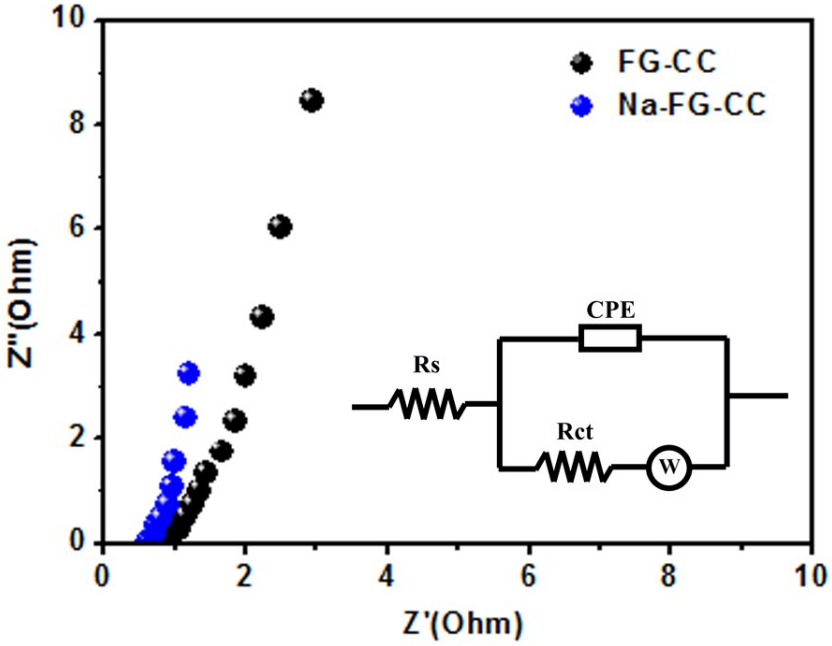

Fig.S9 Nyquist plots of the FG-CC and Na-FG-CC

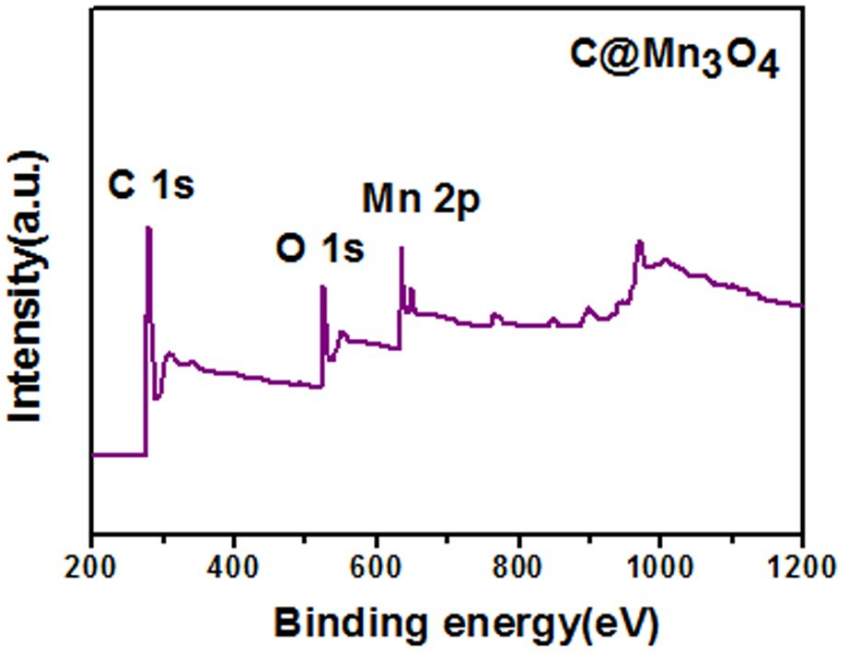

Fig.S10 The XPS survey scan spectra of the C@Mn_3O_4 nanoparticles

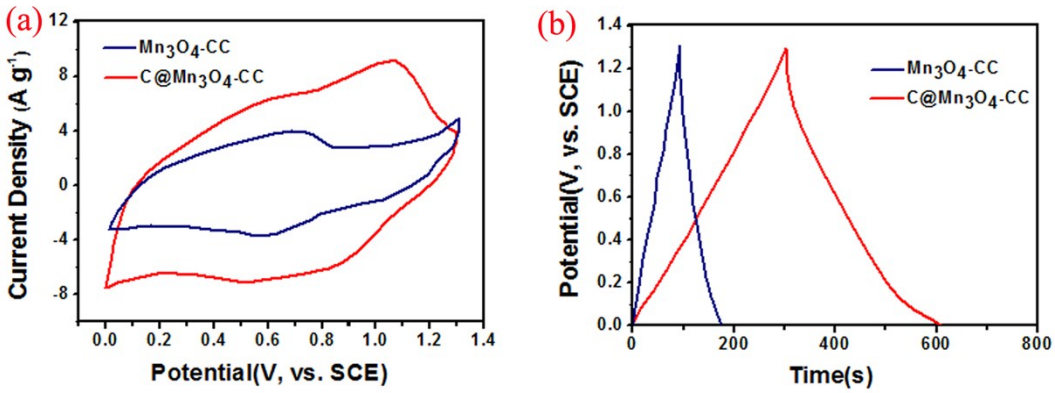

Fig.S11 Comparative CV curve of Mn_3O_4-CC and C@ Mn_3O_4-CC at 50 mV s^{-1} (a), Comparative GCD curve of Mn_3O_4-CC and C@ Mn_3O_4-CC at 1.5 A g^{-1} (b)

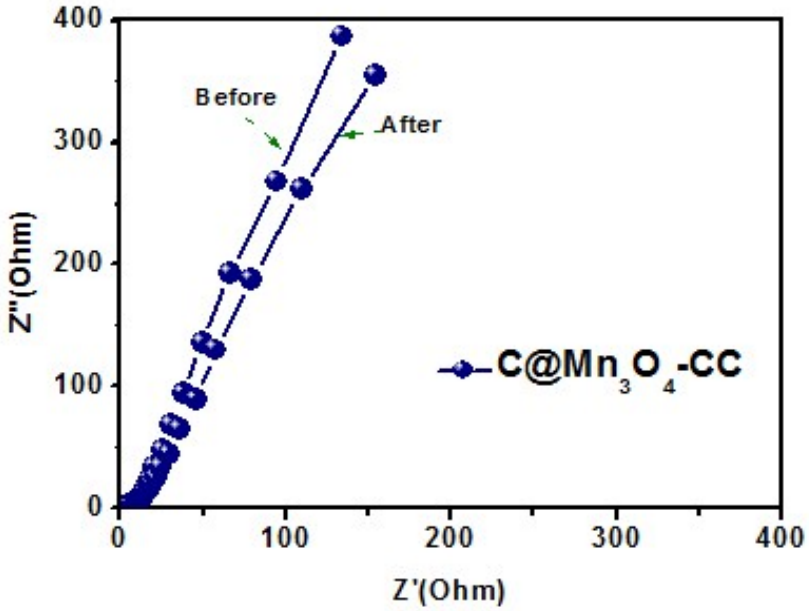

Fig.S12 Nyquist plots of the before and after cycles C@ Mn_3O_4-CC

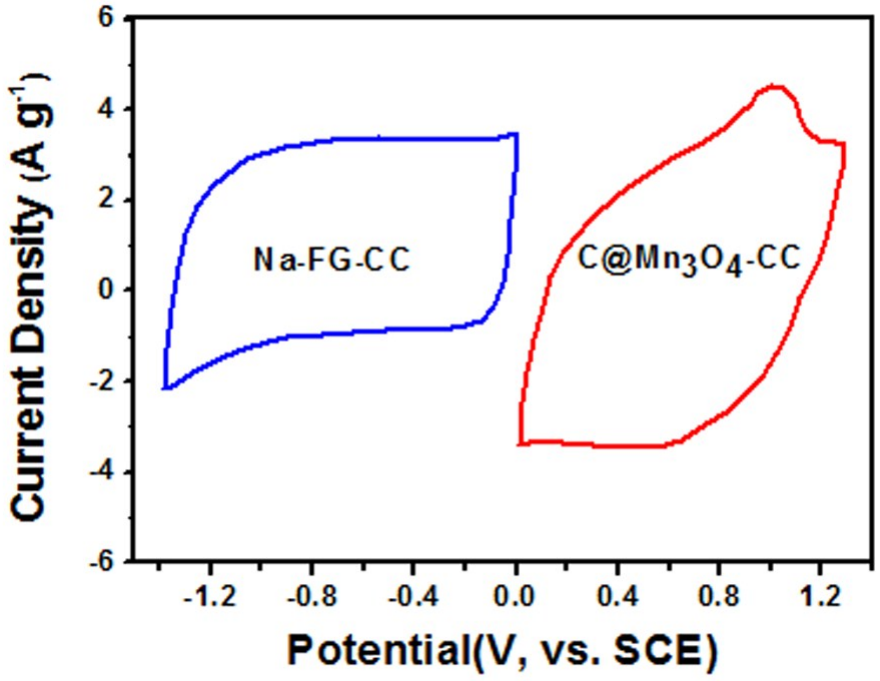

Fig.S13 CV curves of the Na-FG-CC and the C@Mn_3O_4-CC electrodes in separate potential windows at a scan rate of 20 mV s^{-1}

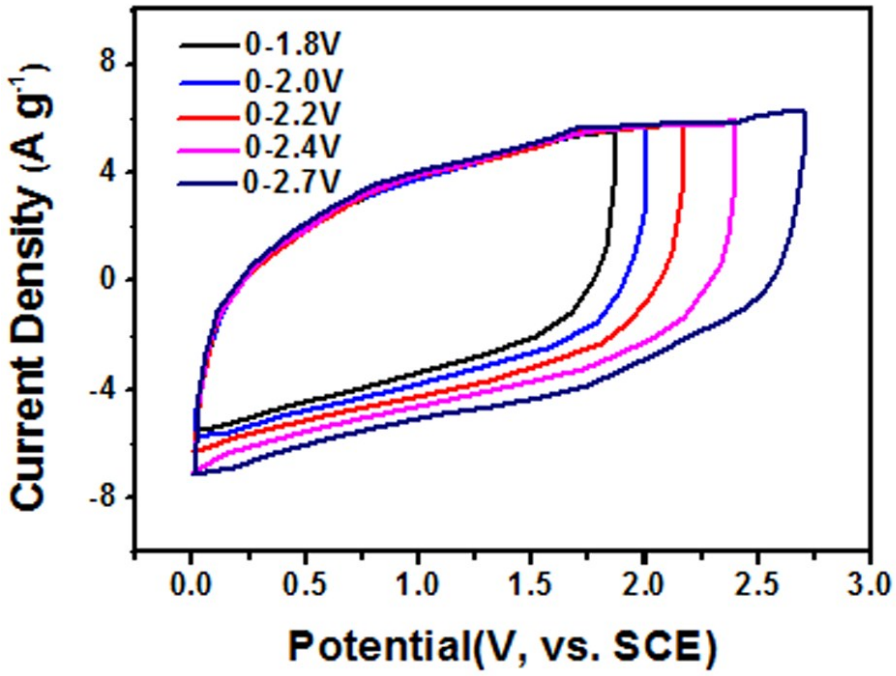

Fig.S14 CV curves of the Na-FG-CC//C@Mn_3O_4-CC asymmetric supercapacitor in different potential windows at a scan rate of 50 mV s^{-1}

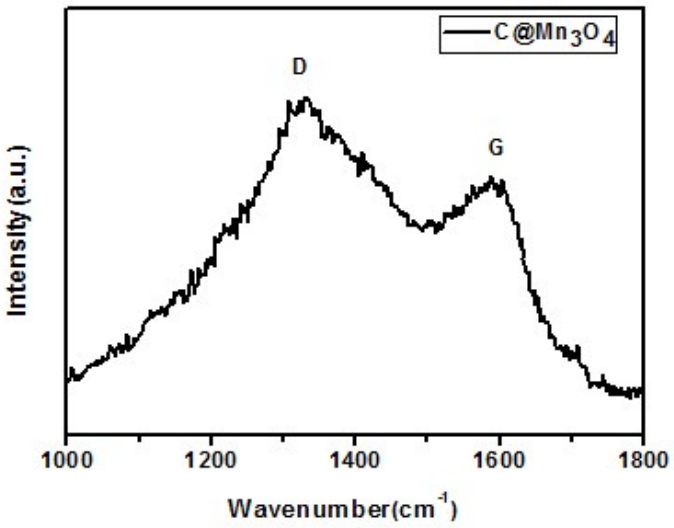

Fig.S15 Raman spectrum of the $C@Mn_3O_4$

The carbon layer was further characterized by Raman measurements. From the Fig,S15, the two major Raman bands located at 1332 and 1600 cm^{-1}. The band at 1332 cm^{-1} corresponds to the D peak arising from the breathing motion of sp^2 rings, and the band at 1600 cm^{-1} was in good agreement with the G band. The ration between the D and G bands was found to be correlated to the nature of carbon. The measured intensity I_D/I_G ration was about 1.33, suggesting that the carbon layer existed in a disordered graphitic form.

Table.S2 Fitting values of *F*, *E*, and *P* of Na-FG-CC using the equation (1-3)

I	Δt	ΔU	***F***	***E***	***P***
1.0	399	1.4	**285**	**77.5**	**699**
2.0	174	1.4	**249**	**67.5**	**1396.5**
5.0	60	1.4	**215**	**58.3**	**3498**
10	27	1.4	**193**	**52.5**	**7000**
20	11.4	1.4	**164**	**44.3**	**13989**
50	4.3	1.4	**154**	**41.8**	**34995**

Units: *I*: A g^{-1}; Δt : s; *F*: F g^{-1}; *E*: Wh kg^{-1}; *P*: W kg^{-1}

Table.S3 Fitting values of *F*, *E*, and *P* of C@Mn_3O_4-CC using the equation (1-3)

I	Δt	ΔU	***F***	***E***	***P***
0.5	826	1.3	**318**	**74.5**	**325**
1.0	367	1.3	**283**	**66.2**	**650**
2.0	169	1.3	**260**	**61**	**1299**
5.0	63.4	1.3	**244**	**57.3**	**3250**
10	30.4	1.3	**234**	**54.9**	**6501**

Units: *I:* A g^{-1} ; Δt : s; *F*: F g^{-1}; *E*: Wh kg^{-1}; *P*: W kg^{-1}

Table.S4 Fitting values of *F*, *E*, and *P* of asymmetric aqueous-supercapacitor using the equation (1-3)

I	Δt	ΔU	***F***	***E***	***P***
1.0	294	2.7	**109**	**110.4**	**1352**
2.0	120	2.7	**89**	**90**	**2703**
5.0	39.4	2.7	**73**	**73.9**	**6753**
10	17.3	2.7	**64**	**64.8**	**13484**
20	7.7	2.7	**57**	**57.7**	**26982**

Units: *I:* A g^{-1} ; Δt : s; *F*: F g^{-1}; *E*: Wh kg^{-1}; *P*: W kg^{-1}

Table.S5 Comparison study on the electrochemical performance of asymmetric aqueous-supercapacitor in this work with previously reported results

Active materials	**Electrolyte**	**Potential**	***F*(F g^{-1})**	***E*(W h kg^{-1})**	***P*(W kg^{-1})**	**Capacitance retention**	**Ref.**
MnO_x/CF// MnO_x/carbon nanofibers	1 M Na_2SO_4	0~1.8V	82	18	11000	94 % after 5000 cycles	[1]
MnO_2/GO//porous	1 M Na_2SO4	0~2V	--	46.7	2000	93% after	[2]

carbon						4000 cycles	
CF/MnO_2// AC	1 M Na2SO4	0~2v	57	36.7	7700	92 % after 10000 cycles	[3]
MnO_2/PANI//AC	PVA/ Na_2SO_4	0~1.7V	100.2	40.2	6300	--	[4]
rGO/MnOx//AC	$[C_2MIm]BF_4$	0~2.7V	47.3	29.7	20800	96% after 8000 cycles	[5]
MnO_2@CNT//MoO_3@CNT	1 M Na_2SO_4	0~2V	--	27.8	10000	96.8% after 10000 cycles	[6]
$Na_{0.25}MnO_2$//ERPC	1 M Na_2SO_4	0~2.7V	82.9	61.1	982.5	93.7% after 10000 cycles	[7]
PPy/MnO_2// AC	1 M Na_2SO_4	0~1.8V	57	25.8	9000	90.3% after 6000 cycles	[8]
CNT/MnO_2//CNT/PPy	0.5M Na_2SO_4	0~1.6V	--	22.8	2700	--	[9]
Graphene/MnO_2 //Graphene/MoO_3	1 M Na_2SO_4	0~2V	--	42.6	276	--	[10]
Porous carbon //MnO_2/carbon	1 M Na_2SO_4	0~2V	--	63.5	8000	93.4% after 5000 cycles	[11]
Mn_3O_4 //NC	6 M KOH	0~1.5V	--	17.276	207.3	100% after 5000 cycles	[12]
Ni@MnO_2//Ni@Fe_2O_3	1M Na_2SO_4	0~1.6V	--	34.1	3197.7	--	[13]
3D MnO_2//AC	1 M Na_2SO_4	0~1.7V	--	40.2	6227	90% after 8000 cycles	[14]
Mn_3O_4/carbon// AC	1 M Na_2SO_4	0~2V	--	19	4500	95% after 5000 cycles	[15]
$Na_{0.5}MnO_2$//Fe_3O_4@C	1 M Na2SO4	0~2.6V	88	81	2000	--	[16]

					0		
$MnCO_3$//Carbon	2M KOH	0~1.6V	48.4	14.7	3300	97.3% after 10000 cycles	[17]
rGO@Mn_3O_4//rGO@VO2	1 M Na_2SO_4	0~2.2V	--	42.7	11260	--	[18]
Graphene-MnO_2//graphene	1 M Na_2SO_4	0~2V	--	30	5000	79% after 1000 cycles	[19]
α-MnO_2//α-MnO_2	1 M Na_2SO_4	0~0.8V	--	20.8	3200	--	[20]
Na-FG-CC/C@Mn_3O_4-CC	**1M Na_2SO_4**	**0~2.7**	**109**	**110.4**	**26982**	**96% after 10000 cycles**	**This work**

Reference

[1] H. Wang, J. Deng, Y. Chen, F. Xu, Z. Wei, Y. Wang, Hydrothermal synthesis of manganese oxide encapsulated multiporous carbon nanofibers for supercapacitors ***Nano Res***, 2016, 9, 2672.

[2] Zhao, Y.; Ran, W.; He, J.; Huang, Y.; Liu, Z.; Liu, W.; Tang, Y.; Zhang, L.; Gao, D.; Gao, F., High-Performance Asymmetric Supercapacitors Based on Multilayer MnO_2/Graphene Oxide Nanoflakes and Hierarchical Porous Carbon with Enhanced Cycling Stability. ***Small***, 2015, 11, 1310-1319.

[3] S. C. Lin, Y. T. Lu, Y. A. Chien, J. A. Wang, T. H. You, Y. S. Wang, C. W. Lin, C. C. M. Ma, C. C. Hu, J. Asymmetric supercapacitors based on functional electrospun carbon nanofiber/manganese oxide electrodes with high power density and energy density. ***J. Power Sources***, 2017, 362, 258.

[4] N. Liu, Y. Su, Z. Wang, Z. Wang, J. Xia, Y. Chen, Z. Zhao, Q. Li, F. Geng, Electrostatic-Interaction-Assisted Construction of 3D Networks of Manganese Dioxide Nanosheets for Flexible High-Performance Solid-State Asymmetric Supercapacitors. ***ACS Nano***, 2017, 11, 7879.

[5] Y. Wang, W. Lai, N. Wang, Z. Jiang, X. Wang, P. Zou, Z. Lin, H. J. Fan, F. Kang, C. P. Wong, C. Yang,Reduced Graphene Oxide/Mixed-valent Manganese Oxides

Composite Electrode for Tailorable and Surface Mountable Supercapacitors with High Capacitance and Super-Long Life. ***Energy Environ. Sci***, 2017, 10, 941.

[6] Lee, T. H.; Pham, D. T.; Sahoo, R.; Seok, J.; Luu, T. H. T.; Lee, Y. H. High Energy Density and Enhanced Stability of Asymmetric Supercapacitors with Mesoporous MnO_2@CNT and Nanodot MoO_3@CNT Free-Standing Films. ***Energy Storage Mater***, 2018, 12, 223-231.

[7] Ting X., Teck L.T., Li L., Wee S.V. L., Junmin X. Harmonizing Energy and Power Density toward 2.7 V Asymmetric Aqueous Supercapacitor. ***Adv. Energy Mater.*** 2018, 8, 1702630.

[8] W. He, C. Wang, F. Zhuge, X. Deng, X. Xu, T. Zhai, Flexible and high energy density asymmetrical supercapacitors based on core/shell conducting polymer nanowires/manganese dioxide nanoflakes. ***Nano Energy***, 2017, 35, 242.

[9] Liu, J., Zhang, L., Wu, H.B., Lin, J., Shen, Z., Lou, X.W. High-Performance Flexible Asymmetric Supercapacitors Based on A New Graphene Foam/Carbon Nanotube Hybrid Film. ***Energy Environ. Sci,.*** 2014, 7, 3709-3719.

[10] Chang, J.; Jin, M.; Yao, F.; Kim, T. H.; Le, V. T.; Yue, H.; Gunes, F.; Li, B.; Ghosh, A.; Xie, S.; Lee, Y. H. Asymmetric Supercapacitors Based on Graphene/MnO_2 Nanospheres and Graphene/MoO_3 Nanosheets with High Energy Density. ***Adv. Funct. Mater***, 2013, 23, 5074- 5083.

[11] X. Wu, L. Jiang, C. Long, Z. Fan, From flour to honeycomb-like carbon foam: Carbon makes room for high energy density supercapacitors. ***Nano Energy***, 2015, 13, 527.

[12] Wang, G.; Ma, Z.; Fan, Y.; Shao, G.; Kong, L.; Gao, W. Preparation of Size-Selective Mn_3O_4 Hexagonal Nanoplates with Superior Electrochemical Properties for Pseudocapacitors. ***Phy. Chem. Chem. Phys***, 2015, 17, 23017-23025.

[13] Li, Y.; Xu, J.;Feng,T.; Yao,Q.; Xie, J.; Xia, H. Fe_2O_3 Nanoneedles on Ultrafine Nickel Nanotube Arrays as Efficient Anode for High-Performance Asymmetric Supercapacitors. ***Adv. Func. Mater***, 2017, 27, 1606728.

[14] Liu, N.; Su, Y.; Wang, Z.; Wang, Z.; Xia, J.; Chen, Y.; Zhao, Z.; Li, Q.; Geng,F. Electrostatic-Interaction-Assisted Construction of 3D Networks of Manganese

Dioxide Nanosheets for Flexible High-Performance Solid-State Asymmetric Supercapacitors. ***ACS Nano***, 2017, 11, 7879-7888.

[15] K. Makgopa, K. Raju, P. M. Ejikeme, K. I. Ozoemena, High-performance Mn3O4/onion-like carbon (OLC) nanohybrid pseudocapacitor: Unravelling the intrinsic properties of OLC against other carbon supports. ***Carbon***, 2017, 117, 20.

[16] Nawishta J., Ahmad H., Qiuying X., Shuo S., Junwu Z., Hui X. High-Performance 2.6 V Aqueous Asymmetric Supercapacitors based on In Situ Formed $Na_{0.5}MnO_2$ Nanosheet Assembled Nanowall Arrays. ***Adv. Mater.***, 2017, 29, 1700804.

[17] Y. Tang, S. Chen, T. Chen, W. Guo, Y. Li, S. Mu, S. Yu, Y. Zhao, F. Wen, F. Gao, Synthesis of peanut-like hierarchical manganese carbonate microcrystals via magnetically driven self-assembly for high performance asymmetric supercapacitors. ***J. Mater. Chem. A***, 2017, 5, 3923.

[18] R. Sahoo, D.T. Pham, T.H. Lee, T.H.T. Luu, J. Seok, Y.H. Lee，Redox-Driven Route for Widening Voltage Window in Asymmetric Supercapacitor. ***ACS Nano***，2018, 12, 8494.

[19] Wu, Z.S., Ren, W., Wang, D.W., Li, F., Liu, B., Cheng, H.M. High-Energy MnO_2 Nanowire/Graphene and Graphene Asymmetric Electrochemical Capacitors. ***ACS Nano***, 2010, 4, 5835.

[20] B. Z. Yu, X. D. Zhao, J. Luo, H. G. Zhang, Y. W. Zhu, G. Y. Jing, P. Ma, Z. Y. Ren, H. M. Fan, Hierarchical α-MnO_2 Tube-on-Tube Arrays with Superior, Structure-Dependent Pseudocapacitor Performance Synthesized via a Selective Dissolution and Coherent Growth Mechanism. ***Adv. Mater. Interfaces***, 2016, 3, 1500761.